Anal. Bioanal. Electrochem., Vol. 17, No. 6, 2025, 497-514
https://www.doi.org/10.22034/abec.2025.725969

Analytical & Bioanalytical Electrochemistry

Full Paper

A Novel Laser Technology Photobiomodulation-Assisted Electrochemical Approach for Hemoglobin Evaluation and Anemia Treatment using MXene/Ni/Sm-LDH Nanocomposite

Sarah Z. Najimaldeen,[1] and Hayder J. Abdulrahman[2,*]

[1]*College of Medicine, Department of Physiology, Kirkuk University, Kirkuk, Iraq*
[2]*College of Dentistry, Department of Basic Sciences, Kirkuk University, Kirkuk, Iraq*

*Corresponding Author, Tel.: +9647710367700
E-Mail: hyder.baban@uokirkuk.edu.iq

Received: 4 June 2025 / Received in revised form: 5 July 2025 /
Accepted: 5 July 2025 / Published online: 7 July 2025

Abstract- This study introduces a dual-function platform that integrates photobiomodulation therapy with a highly sensitive MXene/Ni/Sm-LDH-based electrochemical biosensor for the precise evaluation of hemoglobin levels in patients with anemia. The developed biosensor, constructed on a modified glassy carbon electrode, demonstrated outstanding analytical performance with a detection limit of 0.009 nM and a quantification limit of 0.003 nM for hemoglobin using 10 µL blood samples from four individuals (two males and two females) with anemia. Cyclic voltammetry confirmed a robust linear response (R^2 = 0.9961) within a hemoglobin concentration range of 0.01–0.8 nM. Following green laser irradiation at 505 nm for 10 minutes, blood samples exhibited a 13.2% increase in the electrochemical peak current, correlating with improved hemoglobin availability. Rheological assessments revealed a 15% to 20% decrease in blood viscosity, indicating enhanced red blood cell flexibility and flow. Electrochemical impedance spectroscopy showed a reduction in charge transfer resistance from 18 kΩ (unmodified electrode) to 9 kΩ (modified electrode), signifying better conductivity and electron exchange. Stability testing over 60,000 seconds confirmed the biosensor's long-term operational reliability. The observed physiological enhancements are attributed to mitochondrial adenosine triphosphate production and nitric oxide-mediated vasodilation induced by photobiomodulation. This combined diagnostic and therapeutic strategy offers a promising, non-invasive solution for real-time monitoring and management of anemia.

Keywords- Photobiomodulation; Green laser therapy; Electrochemical biosensor; MXene/Ni/Sm-LDH nanocomposite; Hemoglobin detection; Blood viscosity; Non-invasive diagnostics

1. INTRODUCTION

One major advantage in semiconductor lasers lies in their affordability, Anemia is any disease leading to fewer red blood cell numbers or hemoglobin in red blood cells, as contrasted with healthy controls. This imbalance generally indicates fewer body tissues have enough oxygen, leading to symptoms of fatigue and weakness [1,2]. Several factors can cause anemia, some of which include nutritional deficiencies, chronic diseases, cancer therapies, specific infections such as malaria, and genetic diseases that affect hemoglobin or red blood cell formation. In addition to these, anemia can lead to critical health hazards like cardiovascular disease, developmental slowing in children, pregnancy complications, and illness and premature death rates. Iron deficiency anemia alone affects more than 500 million women across the globe according to the World Health Organization, as most of them are especially of childbearing age and therefore subject to the physical stresses of pregnancy [3]. Diagnosing anemia typically involves measuring hemoglobin levels or hematocrit values through blood tests [4]. This disease infects roughly one quarter of the humans across the globe, and females and pre-pubescent children are most at risk. Hemoglobin in itself is made of a molecule in red blood cells in nearly all mammals and is made up of four globin chains held together by four sets of heme groups. Its general task is to transport oxygen throughout the body. Abnormalities in hemoglobin concentration are often linked to a range of diseases, including anemia, leukemia, kidney disorders, diabetic complications, vascular conditions, and hemoglobinuria. The criteria for low blood hemoglobin concentration are presented in Table 1 [5].

Table 1. Criteria for low blood hemoglobin concentration

Category	Hemoglobin Level
Male Adult	<13 g/dL
Female Adult	<12 g/dL
Age 6–16 Years	<12 g/dL
Age 6 Months–6 Years	<11 g/dL
Pregnancy	<11 g/dL

Modern anemia management encompasses a range of innovative therapies tailored to specific causes and patient needs. Advanced oral iron supplements like ferric maltol and sucrosomial iron have improved gastrointestinal tolerability and absorption, yet may still be inadequate for individuals with severe deficiencies or malabsorption issues. Intravenous iron formulations, such as ferric carboxymaltose, offer rapid replenishment of iron stores but carry risks of infusion reactions and require clinical monitoring. Erythropoiesis-stimulating agents

(ESAs) are effective for chronic kidney disease-related anemia but may increase cardiovascular risks and are costly. Gene therapies, including CRISPR-based approaches like CTX001, show promise for hereditary anemias but are still experimental and expensive. Artificial intelligence systems, such as AISACS, assist in optimizing anemia treatment in hemodialysis patients but depend on high-quality data and infrastructure. Machine learning models like HgbNet enable non-invasive anemia prediction from electronic health records, though their accuracy can be affected by data irregularities [6].

Today, photobiomodulation therapy, utilizing low-level laser light, has emerged as a supportive treatment for anemia. It can enhance red blood cell function, improve oxygen delivery, and stimulate hematopoiesis, offering a non-invasive adjunct to traditional therapies. While not a standalone cure, it holds potential for improving patient outcomes when integrated into comprehensive anemia management plans [7].

Evaluation of hemoglobin in laser therapy-anemic patients uses several methods with certain advantages and limitations. CBC test is the traditional technique, which provides detailed information regarding hemoglobin and other blood components, but it requires venous sampling of blood and may reflect late effects after therapy. Spectrophotometry for hemoglobin gives rapid results using capillary blood but may be affected by some substances and may lead to inaccuracy. Pulse CO-oximetry gives non-invasive, real-time hemoglobin monitoring but may be affected in conditions of decreased perfusion or patient movement. Near-infrared spectroscopy only estimates tissue oxygenation and hemoglobin saturation but has limitations in the form of skin pigmentation and inability to estimate absolute hemoglobin concentrations [8,9].

Electrochemical biosensors hold promise as they can detect hemoglobin levels with very high sensitivity and specificiy but remain in the developmental stage and are thus yet not generally used in the clinic. Therefore, electrochemical methods are especially useful in this investigation because they can potentially be used in real time and at the point-of-care for hemoglobin level monitoring, which will be important in determining the effectiveness of laser therapy in anemia treatment. Because they are highly sensitive and specific, they can identify the very small changes in hemoglobin levels, which can facilitate early clinical decisions. They can become standard in individualized approaches for managing anemia as technology further develops [1,10].

In this study, MXene-based nanocomposites were synthesized for the detection of hemoglobin in pre- and post-treatment samples of anemic patients. This is the first study to use MXene-based nanocomposites for determining hemoglobin levels. Parameter optimization was performed on standard and laser-irradiated blood samples of anemic patients. Then, the effects of laser irradiation on the improvement of anemia and the relationship between the rheology (fluidity) properties of patients' blood and the amount of hemoglobin protein in their blood were studied and analyzed.

2. EXPERIMENTAL SECTION

2.1. Material

High-purity graphite powder (particle size below 45 μm, 99.99% trace metals basis), titanium powder (particle size <45 μm, 99.98% purity), potassium ferricyanide, aluminum powder (60 μm, 99.9% purity), potassium chloride, uric acid, carbon-based ink, and samarium(III) chloride ($SmCl_3$, 99.9% purity, powdered form) were purchased from Sigma-Aldrich. Additionally, *L*-ascorbic acid, *D*-fructose, and urea of analytical grade were obtained from Supelco-Sigma-Aldrich. Sodium chloride, potassium hydroxide pellets, and nickel(II) chloride hexahydrate ($NiCl_2 \cdot 6H_2O$) were provided by Merck. Polyvinylpyrrolidone (PVP K30), PIL-1, and chitosan, which served as conductive binding agents, were sourced from Merck-Millipore. The phosphate salts, potassium hydrogen phosphate (K_2HPO_4) and potassium dihydrogen phosphate (KH_2PO_4), were acquired from Neutron Co. Human serum samples were purchased from Sigma-Aldrich. Additionally, human blood samples used in this study were obtained from four individuals (two males and two females) with anemia. Blood specimens were collected using dipotassium ethylenediaminetetraacetic acid (K_2-EDTA) tubes (BD Vacutainer) following informed consent from each participant. Prior to beginning the study, formal authorization was obtained from the Ethics Board of the Medical University and Hospital in Kirkuk.

2.2. Synthesis Methods and Preparation

2.2.1. Preparation of MXene/Ni/Sm-LDH

A hydrothermal in situ synthesis was used to fabricate the MXene/nickel/samarium layered double hydroxide (MXene/Ni/Sm-LDH) nanocomposite. Initially, a mixture containing 0.162 g of MXene (prepared as described in previous work [11]), 0.3 g of $NiCl_2 \cdot 6H_2O$, 0.15 g of $SmCl_3$, and 2.4 g of urea was dispersed in 200 mL of deionized water under continuous stirring at room temperature. This homogeneous solution was then sealed in an autoclave and subjected to hydrothermal processing at 120 °C for 12 hours. After the reaction, the resulting material was collected, thoroughly rinsed several times with deionized water to remove any residual impurities, and subsequently dried in a vacuum oven at 70 °C.

2.2.2. Construction of the Electrochemical Biosensor

To fabricate the electrochemical biosensor, 0.06 g of the prepared MXene/Ni/Sm-LDH composite was mixed with 0.09 g of PVP in 4 mL of deionized water. This mixture was stirred for 30 minutes to ensure uniform dispersion. A glassy carbon electrode (GCE, 2 mm diameter) was carefully polished using a 0.05 μm alumina slurry and then rinsed thoroughly with deionized water. Subsequently, 1 μL of the composite solution was applied onto the electrode

surface using a micropipette. The modified electrode was left to air dry at room temperature for 30 minutes before further use [11].

2.3. Characterization

Elemental structure and surface morphology of the deposited MXene material, in this instance, $Ti_3C_2(OH)_2$, were determined by using field emission scanning electron microscope (FESEM, TESCAN MIRA3) and transmission electron microscopy (TEM). Phase detection was conducted using X-ray diffraction (XRD) analysis using a PHILIPS PW1730 system, which operated in the 2θ region between 10° and 80°. Additionally, functional groups were determined using Fourier-transform infrared (FTIR) spectroscopy (Bruker ALPHA II). Electrochemical response, i.e., cyclic voltammetry (CV) and electrochemical impedance spectroscopy (EIS), were conducted using the three-electrode system and AUTOLAB PGSTAT204 potentiostat. Here, the glassy carbon and silver/silver chloride (Ag/AgCl) and platinum wire were utilized as working, reference, and counter electrodes, respectively. Impedance study was conducted in the frequency region between 100 kHz and 1 MHz using 10 mV.

Blood samples were collected from all participants so that hematocrit levels were determined using capillary tubes. One end of each capillary tube was sealed with wax, and one sample was irradiated for 10 minutes using a neodymium-doped yttrium aluminum garnet (Nd:YAG) laser. Both samples were then, respectively, centrifuged at 3000 rpm for 10 minutes in an attempt to segregate the components. After being centrifuged, the capillary tubes were carefully removed and the volume of red blood cell packing determined using an electrochemical hemoglobin (Hi) biosensor in a bid to determine the level of anemia in both the irradiated and controlled samples. This was done in both male and female participants so as to ensure consistency and reliability in the findings [12,13].

The major benefits of semiconductor lasers include their affordability in terms of price and availability and their safety in steady state or CW operation so as to not offer severe hazards in normal use. The active medium consists of a prudent mixture of neodymium (Nd) and yttrium aluminum garnet (YAG) crystals in 10:1 ratio, which are hosted in a sealed glass tube approximately 10–80 cm in length and 2–10 mm in diameter and kept in controlled pressure in the range 8–12 Torr. One significant characteristic of this system that caught attention is the compact power supply since the laser can operate with very minimal electrical input. Its wavelength when it luminesces is 505 nm and therefore lies in the green part of the visible spectrum [14,15].

3. RESULTS AND DISCUSSION

3.1. Characterization of MXene based Nanocomposite

The structural phase, surface morphology, and elemental composition of the MAX phase, MXene, and the MXene/Ni/Sm–LDH nanocomposite were systematically investigated using X-ray diffraction, field-emission scanning electron microscopy, and energy-dispersive X-ray spectroscopy (EDS). To investigate the structural characteristics of the synthesized nanocomposites, X-ray diffraction analysis was conducted, with the resulting patterns presented in Figure 1.

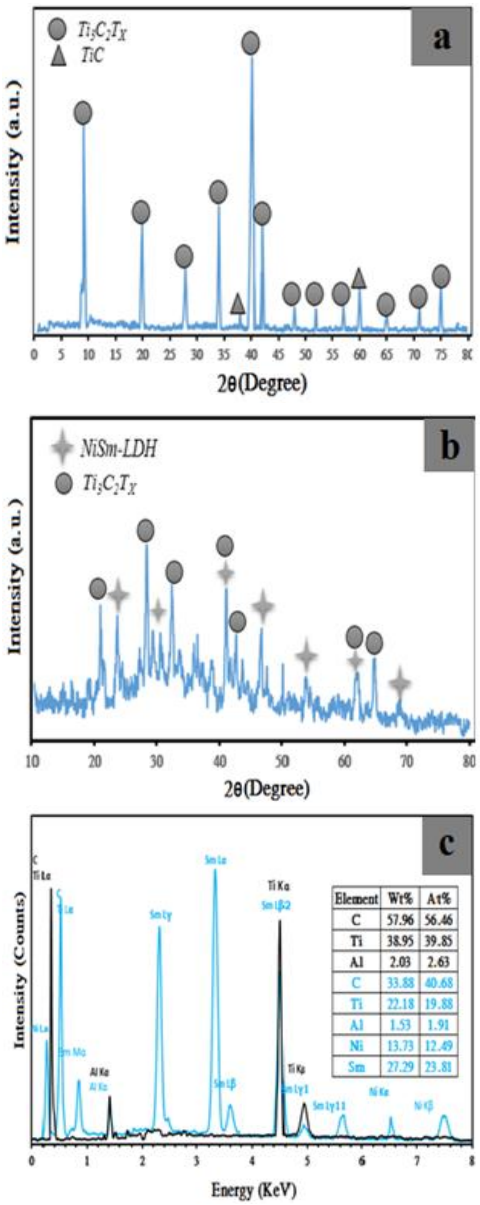

Figure 1. XRD of (a) $Ti_3C_2T_X$ and (b) $Ti_3C_2T_X$/Ni/Sm; (c) EDS of $Ti_3C_2T_X$ (black line) and $Ti_3C_2T_X$/Ni/Sm (light blue line)

The diffraction data revealed two distinct peaks at approximately 9.2° and 40.65°, which were attributed to the presence of $Ti_3C_2(OH)_2$, as shown in Figure 1a. Meanwhile, the prominent diffraction peaks observed at 23.8°, 29.2°, and 41.63° confirmed the successful

formation of Ni/Sm-LDH structures (Figure 1b). Energy-dispersive X-ray spectroscopy analysis further verified the incorporation of samarium and nickel into the material, as depicted in Figure 1c. Additionally, the analysis confirmed a significant reduction in aluminum content, likely due to the alkaline etching of the MAX phase during synthesis. Representative field-emission scanning electron microscopy images of the prepared materials are presented in Figure 2a–c. As illustrated in Figure 2a, Ti_3AlC_2 powders exhibit a dense, compact structure. In contrast, Figures 2b and 2d reveal that $Ti_3C_2T_x$ powders feature a characteristic multilayered, sheet-like morphology. Moreover, Figures 2c, 2e, and 2f clearly demonstrate a stacked, layered structure with an even distribution of nickel and samarium nanoparticles across the composite surface. Collectively, these findings validate the successful fabrication of the MXene/Ni/Sm-LDH composite.

As demonstrated by the FTIR spectrum in Figure 3, a noticeable absorption band appears around 3400 cm^{-1}, corresponding to the hydroxyl groups present on the surface of MXene. Following the introduction of nickel and samarium nanoparticles, as shown in Figure 3, the intensity of this band decreased, indicating a reaction between these nanoparticles and the hydroxyl functionalities.

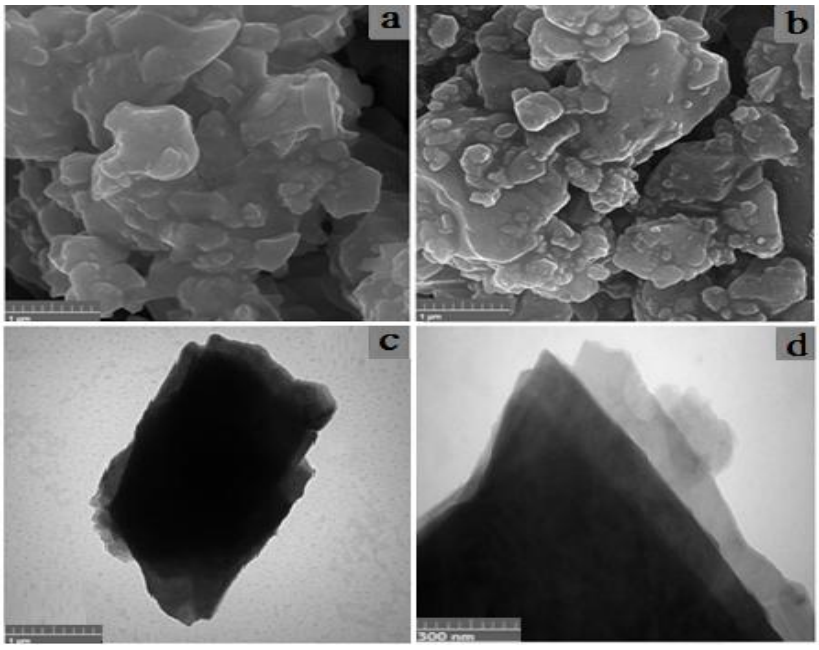

Figure 2. FESEM images of (a) $Ti_3C_2T_X$ and (b) $Ti_3C_2T_X$/Ni/Sm; TEM images of (c) $Ti_3C_2T_X$ and (d) $Ti_3C_2T_X$/Ni/Sm

This suggests that the inherently negative surface charge of MXene enables it to attract and bind positively charged ions, providing ideal anchoring sites for the nucleation of nanomaterials. It can thus be inferred that during the hydrothermal in-situ synthesis process, nickel and samarium ions interact specifically with the -OH groups on the MXene surface.

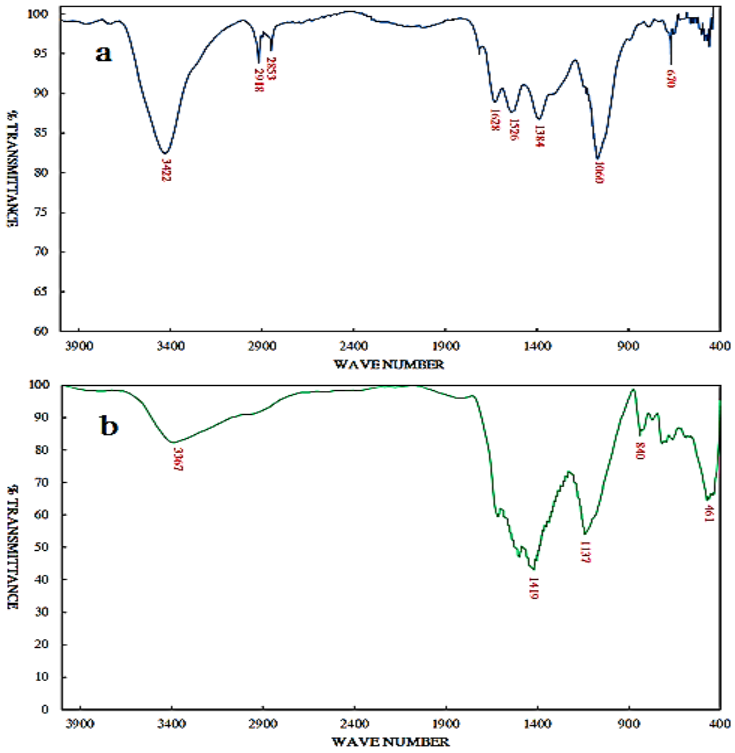

Figure 3. FTIR of (a) $Ti_3C_2T_X$ and (b) $Ti_3C_2T_X$/Ni/Sm

This interaction promotes their immobilization, ultimately leading to the formation of Ni/Sm-LDH nanoparticles at these active sites. These newly formed nanoparticles display strong mechanical adhesion to the substrate and establish effective electrical pathways, thereby enhancing charge-transfer performance.

3.2. Electrochemical Properties of the Electrochemical Biosensor

To begin the investigation of the electrochemical sensing capabilities of the MXene/Ni/Sm-LDH nanocomposite, cyclic voltammetry was employed. The corresponding cyclic voltammetry profiles, illustrated in Figure 4, were recorded using a MXene/Ni/Sm-LDH-modified glassy carbon electrode (MXene/Ni/Sm-LDH/GCE) in a solution of 0.1 M potassium ferrocyanide with 0.1 M KCl as the supporting electrolyte. In Figure 4, the cyclic voltammetry profiles of various electrode configurations are illustrated, comprising bare GCE, GCE modified with MXene, and further modifications incorporating Ni-LDH, Sm-LDH, and a combination of Ni/Sm-LDH on MXene. Among all, the GCE/MXene/Ni/Sm-LDH electrode exhibited a significant enhancement in redox activity, with distinctly elevated anodic and cathodic peak currents occurring at approximately 0.66 V and 0.45 V, respectively. This marked improvement highlights the superior electrocatalytic performance of this electrode, likely due to the cooperative interaction between the d^8 orbitals of Ni and the f^6 orbitals of Sm.

Such synergy appears to greatly facilitate the electron transfer process during the electrochemical oxidation of hemoglobin.

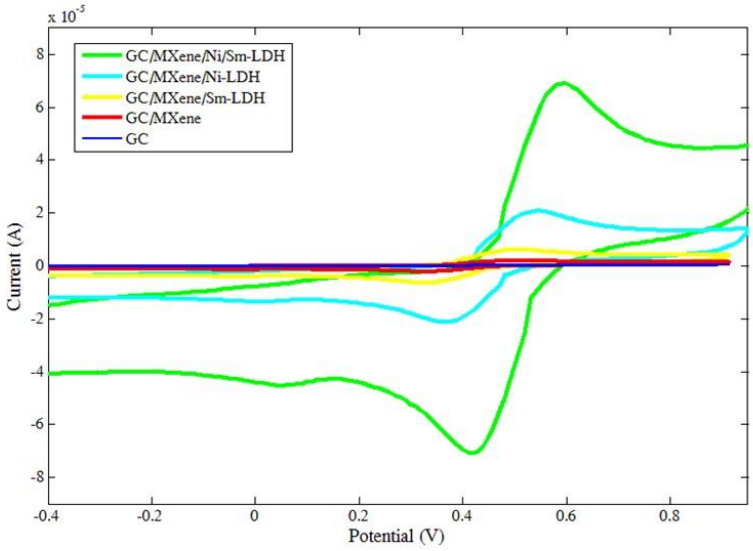

Figure 4. CV curves of different electrodes in 5 mM $K_3Fe(CN)_6/K_4Fe(CN)_6$ (1:1) solution containing 0.1 M KCl at scan rate of 100 mVs^{-1}

The interaction between different concentrations of hemoglobin and the MXene/Ni/Sm-LDH-modified glassy carbon electrode was explored using cyclic voltammetry, as illustrated in Figure 5a. As the hemoglobin concentration increased, a corresponding rise in the oxidation peak current was observed. The most pronounced oxidation peak appeared at a concentration of 0.8 nM, whereas the weakest response was recorded at 0.01 nM. This direct relationship between hemoglobin concentration and current response is quantitatively supported by a high correlation coefficient ($R^2 = 0.9961$), as seen in Figure 5b.

To assess the selectivity of the MXene/Ni/Sm-LDH/GCE for hemoglobin, a study was conducted involving potential interfering agents. Compounds such as albumin, creatinine, glucose, ascorbic acid, glutamine, histidine, tryptophan, and urea — each at a concentration of 0.9 nM — were individually introduced into a hemoglobin solution of the same concentration (0.9 nM). This was done to observe whether these substances would influence hemoglobin detection. Subsequently, a mixed solution containing all the aforementioned species was prepared to simulate a complex environment. Cyclic voltammetry was then employed to analyze the system's electrochemical behavior. The results showed no new peaks in the voltammogram, although a reduction in current intensity was noted (refer to Figure 5c). The sensing mechanism involves a non-enzymatic redox interaction at the MXene/Ni/Sm-LDH/GCE surface, where the Fe^{2+} ion in hemoglobin undergoes a reversible oxidation to Fe^{3+}, facilitated by molecular oxygen through electron transfer:

$$\text{Heme-}Fe^{2+}\text{-}O_2 \leftrightarrow \text{Heme-}Fe^{3+}\text{-}O_2^-$$

The exceptional electrical conductivity of the MXene/Ni/Sm-LDH/GCE significantly improves the efficiency of electron transfer between the electrode interface and hemoglobin molecules. Using this material on a glassy carbon electrode, the detection and quantification capabilities were assessed, resulting in a remarkably low limit of detection (LOD) of 0.009 nM and a limit of quantification (LOQ) of 0.003 nM. For perspective, Table 2 offers a comparative overview, highlighting how the analytical performance of the MXene/Ni/Sm-LDH-modified GCE stacks up against several materials previously documented in the literature.

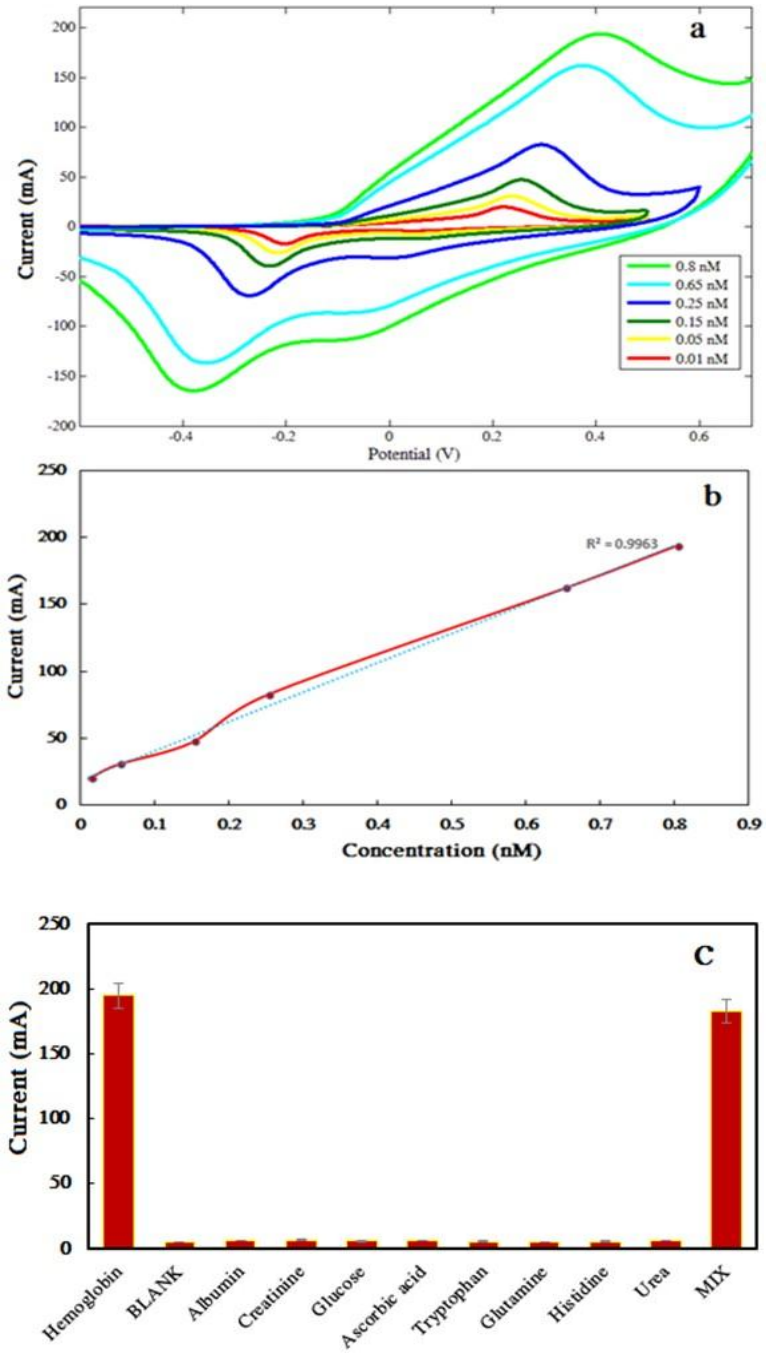

Figure 5. (a) Effect of concentrations of hemoglobin on the current response of cyclic of MXene/Ni/Sm-LDH (c) effect of common interference (0.9 nM) on biosensor performance

Table 2. Comparison of MXene/Ni/Sm-LDH with previously reported materials for hemoglobin sensing

Material	Method	Detection Limit	Linear Range	Ref.
MGCE Modified with Chitosan	Differential pulse voltammetry (DPV)	0.01 μg mL^{-1}	0.05 μg mL^{-1} to 50 μg mL^{-1}	[21]
MIP nanocubes	Cyclic Voltammetry (CV)	0.08 ng mL^{-1}	-	[22]
BDD electrodes modified with platinum	Differential pulse voltammetry	0.0085 nM	0.01 nM–1 nM	[23]
Ferromagnetic CE-Fe-NPs	Cyclic Voltammetry	0.7 pM	-	[24]
MINPs	Differential pulse voltammetry	-	5–100 μg mL^{-1}	[25]
ZnO/GCE	Cyclic Voltammetry	-	25–50 μg mL^{-1}	[26]
CURNPs	Colorimetry	0.1 μg mL^{-1}	1–40 μg mL^{-1}, 150–1200 μg mL^{-1}	[27]
Carbon dots (CDs)	Fluorimetry	0.12 nM	1–4000 nM	[28]
NiTe Nano-rods	Cyclic Voltammetry/Electrochemical Impedance Spectroscopy	0.012 nM	0.9–0.025 nM	[6]
MXene/Ni/Sm-LDH	Cyclic Voltammetry	0.009 nM	0.8–0.01 nM	Present work

One of the key aspects in assessing the performance of a modified electrode is its electrochemical stability. To evaluate this characteristic for the MXene/Ni/Sm-LDH/GCE, cyclic voltammetry was employed using a standard hemoglobin solution (0.8 nM in 1.0 M phosphate-buffered saline, pH 7.4). The experiment was extended to 100 consecutive cycles, and the results—depicted in Figure 6a—demonstrate that the electrode maintains consistent electrochemical behavior throughout, showing negligible variation between the initial, 50th, and 100th cycles. To further assess long-term stability and operational endurance, chronoamperometric analysis was conducted. In this test, the electrode was subjected to a constant potential with a scan rate of 10 mV/s over a duration of 60,000 seconds (as illustrated in Figure 6b). The output current stabilized quickly and remained steady for the entire period, suggesting excellent long-term stability and consistent performance of the MXene/Ni/Sm-LDH/GCE.

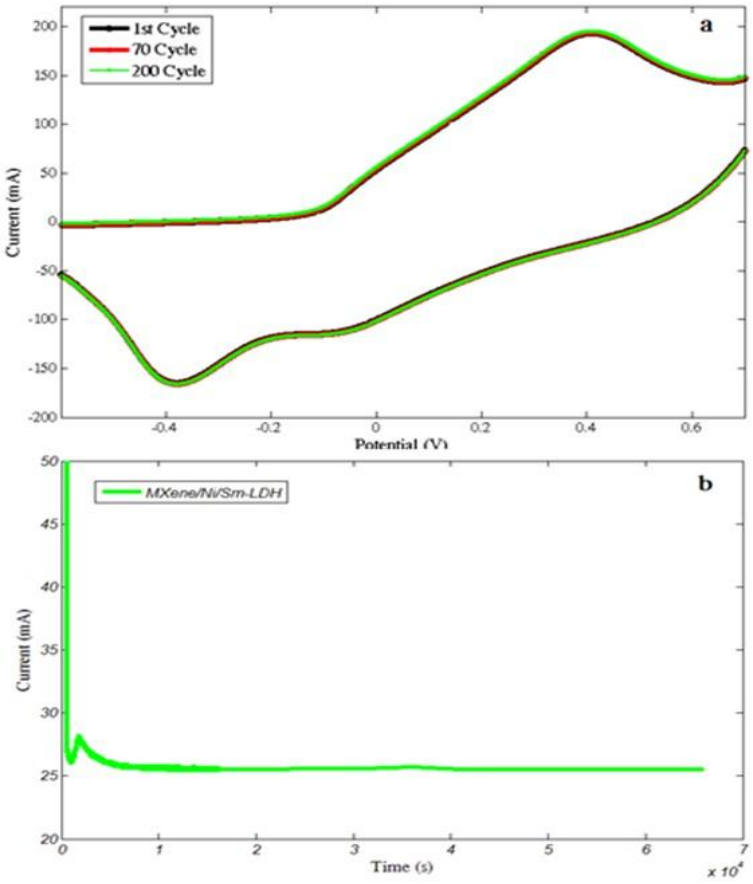

Figure 6. Stability of MXene/Ni/Sm-LDH in 0.8nM hemoglobin solution, (a) Cyclic voltammetry, and (b) Chronoamperometry

Electrochemical impedance spectroscopy was employed using a 0.1 M potassium ferrocyanide solution to investigate the charge-transfer behavior of the MXene/Ni/Sm-LDH/GCE. To benchmark its performance, the bare GCE was also tested under identical conditions (as illustrated in Figure 7a). The impedance profile of the unmodified GCE presented a pronounced semicircular feature, correlating to a charge-transfer resistance (R_{ct}) of approximately 18 kΩ. In contrast, the MXene/Ni/Sm-LDH/GCE exhibited a substantially lower R_{ct} of 9 kΩ, indicating enhanced electron mobility at the electrode-solution interface—attributable to the superior electrical conductivity of the MXene/Ni/Sm-LDH layer. This reduced resistance reflects more efficient charge exchange dynamics.

Further impedance measurements were conducted for various concentrations of hemoglobin using the MXene/Ni/Sm-LDH/GCE (Figure 7b). It was observed that the charge-transfer resistance peaked at the highest hemoglobin concentration (0.8 nM) and progressively declined as the concentration decreased to 0.01 nM. This inverse relationship can be explained by electrostatic interactions between the electrode surface and hemoglobin molecules. Given the relatively large molecular size of hemoglobin, spatial hindrance likely exacerbates resistance at higher concentrations.

The MXene/Ni/Sm-LDH/GCE was ultimately employed to analyze hemoglobin concentrations in whole blood samples collected from patients diagnosed with anemia that were pre- and post-treated with laser irradiation. For this analysis, four distinct blood samples were obtained, each corresponding to a different patient with clinically established hemoglobin levels, as determined using the Abacus 380 hematology analyzer. Electrochemical measurements were carried out via cyclic voltammetry to evaluate the redox behavior of these samples (S1–S5) on the MXene/Ni/Sm-LDH/GCE surface. Among them, the sample labeled S1, originating from a healthy individual, exhibited the most prominent hemoglobin level, as evidenced by a sharp and intense oxidation peak with a relatively high current output.

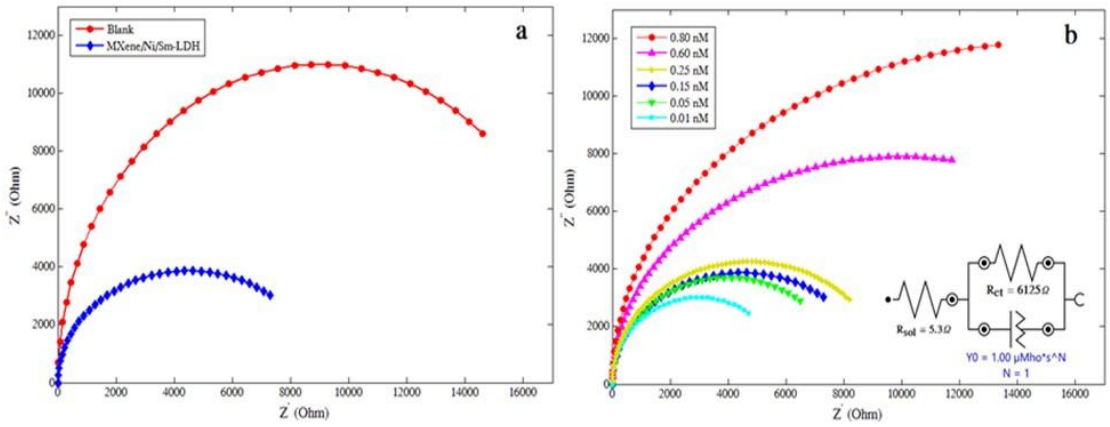

Figure 7. Electrochemical impedance studies for charge-transfer resistance on (a) bare GCE (Blank) and MXene/Ni/Sm-LDH/GCE (b) at different concentrations of hemoglobin

In contrast, samples S2 through S5, which were derived from individuals with progressively lower hemoglobin concentrations, displayed a corresponding decline in oxidation current intensities (Figure 8a). The presence of distinct oxidation and reduction peaks across all samples affirms the significant presence of hemoglobin in these whole blood specimens. The correlation between electrochemical current and hemoglobin concentration is detailed in Table 3. As can be seen from Figure 8b, after laser irradiation of the patient samples, the peak current increased, providing evidence of an increase in hemoglobin concentration and improvement in the patients with anemia. The present work was compared with standard clinical hemoglobin detection methods, and results are presented in Table 4.

In analyzing this behavior, it can be said that laser irradiation of blood samples from patients with anemia has been reported to cause a modest increase in hemoglobin levels or improve the functionality of existing hemoglobin molecules. This effect is not due to the direct production of hemoglobin but rather an enhancement of the physiological environment that supports red blood cell performance and oxygen-carrying capacity. By improving the structural integrity and activity of red blood cells, laser exposure can lead to more efficient oxygen

transport, which may be reflected in improved hemoglobin-related measurements in some studies [16].

Table 3. Blood characteristics of people with anemia, including peak current, hemoglobin concentration and viscosity

Samples	Conc. (nM)	Peak Current (mA)	Viscosity (Cp)
Sample 1	0.74	193	18
Sample 2 post-laser irradiated	0.61	153	27
Sample 3 post-laser irradiated	0.54	121	30
Sample 4 post-laser irradiated	0.45	97	20
Sample 5 post-laser irradiated	0.38	77	17
Sample 2 pre-laser irradiated	0.58	141	30
Sample 3 pre-laser irradiated	0.48	106	35
Sample 4 pre-laser irradiated	0.39	83	24
Sample 5 pre-laser irradiated	0.34	64	20

The underlying cause of these effects is attributed to photobiomodulation. Photobiomodulation may enhance the proliferation of hematopoietic stem cells. When blood is irradiated with low-level laser light, it stimulates cellular components—particularly within the mitochondria—leading to increased adenosine triphosphate (ATP) production and activation of metabolic pathways.

Table 4. Comparison of MXene/Ni/Sm-LDH Biosensor performance with standard clinical hemoglobin detection methods for hemoglobin sensing

Method	Accuracy	Detection limit (molar)	Feasibility
Automated analyzers	CV <1–2%	~0.5 mM	High precision, lab setting, requires trained staff
Point-of-care (HemoCue)	CV ~2–5%	~0.5 mM	Portable, minimal training, field/clinic use
Non-invasive (SpHb)	±1–2 g/dL error	~1 mM	Easy, continuous monitoring, less precise
Electrochemical (Present works)	CV <1–2%	~0.009 nM	High precision, lab setting, Easy and Fast

This process can enhance red blood cell metabolism, reduce oxidative damage, and promote the function of enzymes involved in hemoglobin synthesis and stability. Additionally, laser light, especially in the red (630–660 nm) and green (500–550 nm) ranges, can stimulate bone marrow activity, and laser irradiation may increase erythropoiesis (production of red blood cells, RBCs). Improved blood microcirculation due to nitric oxide release further supports oxygen delivery and may contribute indirectly to better hemoglobin function [16-18].

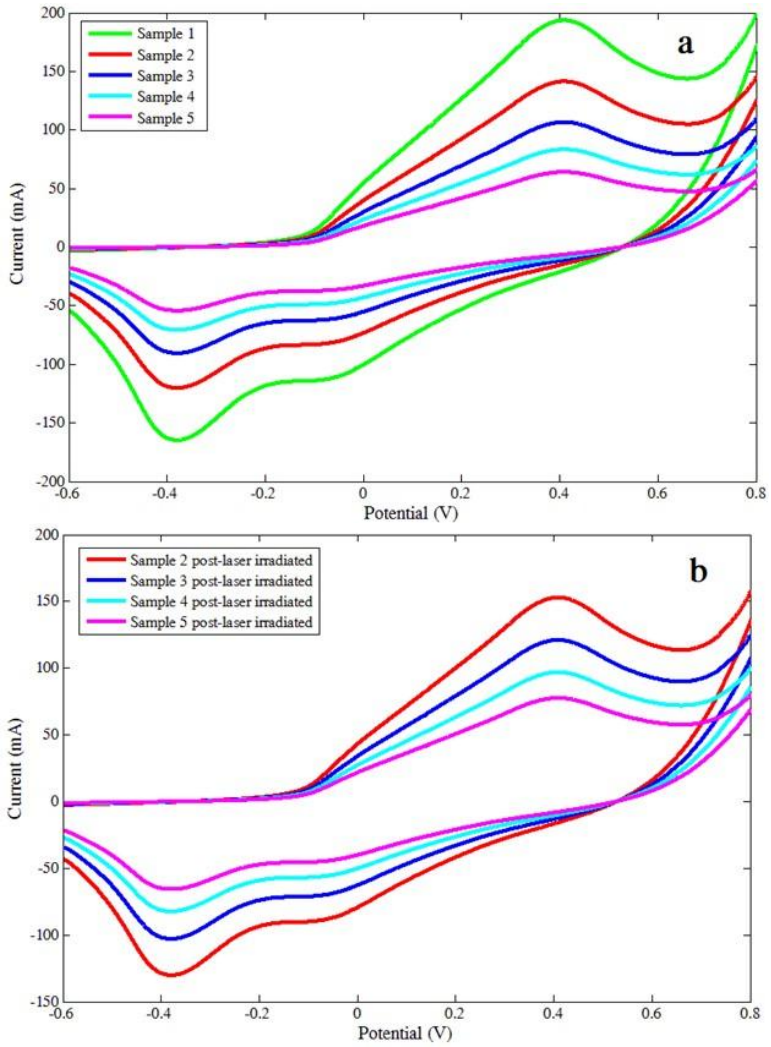

Figure 8. Cyclic voltammetry curves of blood samples of anemic patients by MXene/Ni/Sm-LDH/GCE (a) before irradiation (b) after irradiation by laser

3.3. Effects on Blood Rheology

Therefore, to confirm and investigate the mechanism of the effect of laser irradiation on the improvement of patients with anemia, the rheological properties of the patients' blood were examined. As can be seen from Figure 9 and Table 3, the blood samples exposed to laser irradiation exhibited lower viscosity than the original samples.

Therefore, it can be stated that laser irradiation of blood samples from patients with anemia positively influences the rheological properties and viscosity of blood. Specifically, it can enhance the flexibility and deformability of red blood cells, which are often compromised in anemic conditions. This improvement helps reduce blood viscosity, allowing for smoother flow through the circulatory system. As a result, tissue perfusion and oxygen delivery may be enhanced, which is particularly important in anemia, where oxygen transport is already impaired due to a reduced red blood cell count or hemoglobin levels [19].

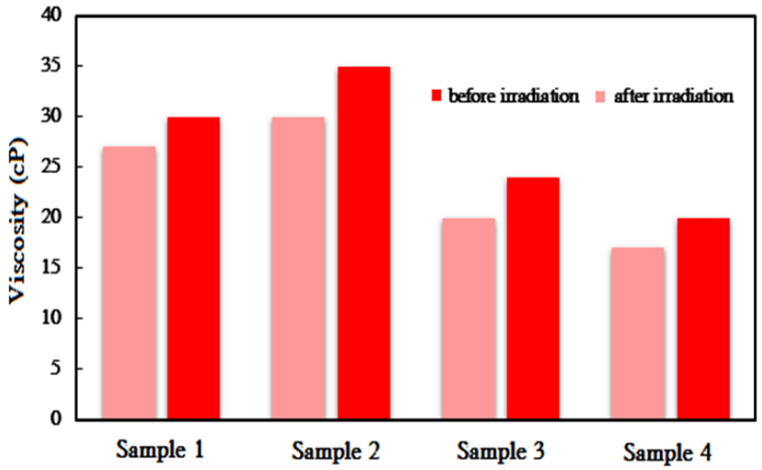

Figure 9. Viscosity changes in anemic patient samples before and after laser irradiation for 10 min

The main cause of these changes lies in a process called photobiomodulation. When blood is exposed to specific wavelengths of low-level laser light, it triggers biochemical reactions within cells, particularly in the mitochondria. These reactions lead to increased production of cellular energy, reduced oxidative stress, and improved membrane stability. Additionally, laser light can promote the release of nitric oxide, which relaxes blood vessels and enhances circulation. Together, these effects contribute to better blood flow characteristics, helping to alleviate some of the functional impairments caused by anemia [20].

4. CONCLUSION

This study presents an innovative integration of photobiomodulation and MXene-based electrochemical biosensing for evaluating and managing anemia. The application of low-level laser therapy demonstrated measurable improvements in hemoglobin levels and blood rheology in anemic patients. Enhanced red blood cell flexibility and reduced blood viscosity were observed, suggesting improved circulatory efficiency. These physiological benefits are primarily attributed to laser-induced mitochondrial activation, which boosts ATP production and redox balance. The newly synthesized MXene/Ni/Sm-LDH nanocomposite biosensor

exhibited high sensitivity and specificity in detecting hemoglobin levels, even in low concentrations. The combined approach not only facilitates non-invasive monitoring but also offers therapeutic potential. The findings support the role of laser irradiation as a valuable adjunct in anemia treatment. Importantly, this dual strategy may offer real-time insights into patient response, enhancing personalized care.

Data availability

Data will be made available on request.

Declaration of Competing interests

The authors declare no competing interests.

REFERENCES

[1] D. Chauhan, R. Gupta, and N. Verma, Electrochim. Acta. 513 (2025) 145603.
[2] R. An, Y. Huang, Y. Man, R.W. Valentine, E. Kucukal, U. Goreke, Z. Sekyonda, C. Piccone, A. Owusu-Ansah, and S. Ahuja, J.A. Little, Lab Chip. 10 (2021) 1843.
[3] M.F. Mohammed, and D.Y. Alsaka, J. Opt. 2025 (2025) 1.
[4] B. Gao, Z. Liang, D. Han, F. Han, W. Fu, W. Wang, Z. Liu, and L. Niu, Talanta 224 (2021) 121924.
[5] H. Cho, S.-R. Lee, and Y. Baek, Sensors 23 (2021) 8043.
[6] B. Fatima, U. Saeed, D. Hussain, S.-e-Z. Jawad, H.S. Rafiq, S. Majeed, S. Manzoor, S.Y. Qadir, M.N. Ashiq, and M. Najam-ul-Haq, Anal. Chim. Acta 1189 (2022) 339204.
[7] G. Tsakanova, A. Avetisyan, E. Karalova, L. Abroyan, L. Hakobyan, A. Semerjyan, N. Karalyan, E. Arakelova, V. Ayvazyan, L. Matevosyan, and A. Navasardyan, Int. J. Mol. Sci. 12 (2022) 6692.
[8] N. Suardi, and J. Ahliya, Allied Medico-Technol. Sci. 2 (2024) 1.
[9] S. Banerjee, S. Sarkar, S. Saha, and S. Karmakar, Proc. SPIE. 12842 (2024) 241.
[10] B.H. Kumar, A. Vaibhav, and P. Srikanth, Indian J. Sci. Technol. 18 (2022) 899.
[11] F. Nasri, M. Hosseini, S.M. Taghdisi, M.R. Ganjali, and M. Ramezani, Microchim. Acta.9 (2024) 506.
[12] H.J. Abdulrahman, and S. Mohammed, J. Nanostruct. 1 (2025) 54.
[13] H.J. Abdulrahman, and S.B. Mohammed, Periódico Tchê Quím. 17 (2020) 1.
[14] A.H. Attallah, F.S. Abdulwahid, H.J. Abdulrahman, A.J. Haider, and Y.A. Ali, Plasmonics. 3 (2025) 1491.
[15] H.J. Abdulrahman, and S.B. Mohammed, J. Nat. Sci. Biol. Med. 15 (2024) 184.
[16] S.B. Mohammed, H.J. Abdulrahman, and A.A. Bazzaz, NeuroQuantology. 7 (2021) 35.

[17] C.H.S. Tonazio, J.B.R. Girondi, R. de Almeida Silva, and S.S. Frison, Photobiomodulation in Wound Care: Evidence for Nursing Practice, Thieme Revinter (2024).
[18] R.S. Shevchenko, V.V. Makarov, S.B. Pavlov, N.M. Babenko, M.V. Kumetchko, O.B. Litvinova, V.V. Komarchuk, Effect of Photobiomodulation Therapy on Reparative Processes of Chronic Wounds at the Remodeling Stage, Archives of the Balkan Medical Union (2024).
[19] T. Walski, K. Grzeszczuk-Kuć, K. Gałecka, N. Trochanowska-Pauk, R. Bohara, A. Czerski, K. Szułdrzyński, W. Królikowski, J. Detyna, and M. Komorowska, Sci. Rep. 1 (2022) 4042.
[20] T.C. dos Santos Malavazzi, L. Andreo, A. Martinelli, M.F.S.D. Rodrigues, A.C.R.T. Horliana, S.K. Bussadori, K.P.S. Fernandes, F.D. Nunes, and R.A. Mesquita-Ferrari, J. Photochem. Photobiol. B 256 (2024) 112921.
[21] Y. Yuan, X. Ni, and Y. Cao, J. Electroanal. Chem. 837 (2019) 219.
[22] I. Pandey, and J.D. Tiwari, Sens. Actuators B 285 (2019) 470.
[23] R. Wulandari, T.A. Ivandini, E. Saepudin, and Y. Einaga, Sens. Mater. 4 (2019) 1105.
[24] E. Matysiak, M. Donten, A. Kowalczyk, M. Bystrzejewski, I.P. Grudzinski, and A.M. Nowicka, Biosens. Bioelectron. 64 (2015) 554.
[25] R. Zhang, S. Xu, J. Luo, and X. Liu, Microchim. Acta 182 (2015) 175.
[26] A. Sagasti, N. Bouropoulos, D. Kouzoudis, A. Panagiotopoulos, E. Topoglidis, and J. Gutierrez, Materials 8 (2017) 849.
[27] N. Pourreza, and H. Golmohammadi, RSC Adv. 3 (2015) 1712.
[28] S. Huang, L. Wang, C. Huang, J. Xie, W. Su, J. Sheng, and Q. Xiao, Sens. Actuators B 221 (2015) 1215.